IEEE Access
Multidisciplinary | Rapid Review | Open Access Journal

Received February 24, 2020, accepted March 8, 2020, date of publication March 11, 2020, date of current version March 20, 2020.

*Digital Object Identifier 10.1109/ACCESS.2020.2980209*

# RF Active Inductors Small-Signal Design by Means of Conformal Transformations

**ALFIERO LEONI[1], (Member, IEEE), VINCENZO STORNELLI[1], (Senior Member, IEEE), LEONARDO PANTOLI[1], (Member, IEEE), GIORGIO LEUZZI[1], AND ZLATICA MARINKOVIC[2], (Senior Member, IEEE)**

[1]Department of Industrial and Information Engineering and Economics, University of L'Aquila, 67100 L'Aquila, Italy
[2]Faculty of Electronic Engineering, University of Niš, 18000 Niš, Serbia

Corresponding author: Vincenzo Stornelli (vincenzo.stornelli@univaq.it)

**ABSTRACT** In this work we present a synthesis method for the design of RF and microwave Active Inductors (AI) based on S-parameters and conformal transformations. The proposed approach allows to study and define the desired AI characteristics directly managing the transfer function of an equivalent two-ports network, thus overcoming the difficulties relative to the characterization of the classical closed-loop architecture that characterizes both the proposed AI architecture and the classical gyrator-C capacitor scheme. By analyzing the obtained AI open-loop transfer function, it is possible to define the design criteria useful to obtain a single port equivalent network showing an inductive behavior at the desired frequency. An example of application of the proposed approach is also provided and the obtained AI is used for the design of a low-power active filter. Measurements are in good agreement with the simulation results, demonstrating the feasibility of the proposed design approach.

**INDEX TERMS** Active inductor, active filter, graph theory, open-loop analysis, synthesis method, S-parameters.

## I. INTRODUCTION

In the integration process of modern RF and microwave systems, some difficulties arise with the use of passive elements and they are due to technology limitations that allow fabricating components with a low-quality factor and high tolerances. In particular, the use of spiral inductors is even more critical because they require a large amount of substrate area and usually entail electromagnetic analysis due to coupling effects. This has aimed the necessity to find suitable alternatives to avoid the general degradation of the system performance. If at higher frequencies it is more manageable, by substituting lumped components with distributed elements, at lower frequencies this solution cannot be pursued without significantly increasing the chip area. So, the definition of suitable alternatives has been necessary, and a promising solution relies on the use of equivalent active inductors. Even if power consuming, active solutions are capable of ensuring high-quality factors and tunability characteristics can also be achieved with respect to passive solutions. Different active inductors have been proposed in the literature [1]–[10], and between them, those based on the Gyrator-Capacitor approach [11] are the more promising for practical applications. This solution is very simple, since an input voltage drives a load capacitor through an inverting transconductance amplifier, thus producing a 90 degree phase shift voltage; this, in turn, drives the output current through a noninverting transconductance providing an inductive behavior from the input terminal (Fig. 1a). Gyrator-C solutions employing differential tunable active inductors (DTAI) [12] or voltage differencing transconductance amplifier (VDTA) [13] have been proposed in the literature, with promising results. However, the schematic complexity, in terms of the number of active and passive components could be disadvantageous, especially for lumped-element discrete RF boards. Starting from the base gyrator-C scheme, an active inductor realized with a single transistor has been already proposed by some of the same Authors and fully investigated in different papers [14]–[20]. It has been conceived with an inverting amplifier, usually realized with a single transistor in common emitter/source configuration, and a passive, feedback network useful to provide the suitable phase delay between the input voltage and

The associate editor coordinating the review of this manuscript and approving it for publication was Yuh-Shyan Hwang.

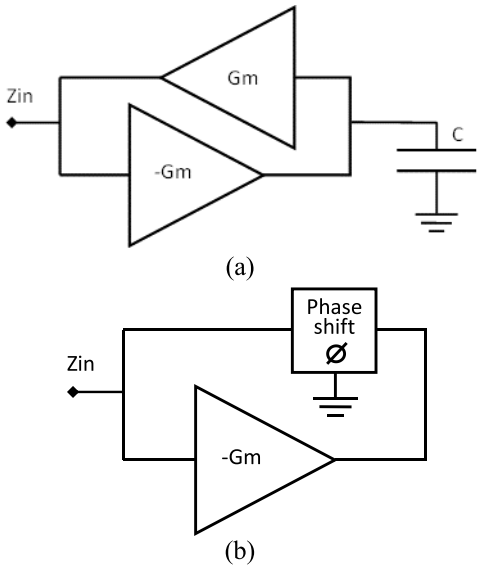


**FIGURE 1.** (a) Gyrator-Capacitor architecture; (b) the active inductor scheme.

the output current. A phase shift of exactly 90 degrees provides an ideal equivalent inductive behavior at the input port of the active network thus conceived (Fig. 1b). This kind of AI (Active Inductor) is generally designed with an optimization process of the network parameters, finalized to obtain the desired inductive behavior. In fact, due to the presence of a feedback network, it is not trivial to define useful design equations, in particular when distributed elements are also included in the design. In addition, the constitutive equations are strictly related to the selected network topologies and so a theoretical formulation of the circuit behavior has never been formalized in real cases.

In this work, we propose a generalized synthesis method for the design of a gyrator-based AI by means of Scattering parameters and conformal transformations. The proposed approach allows determining the general impedance of the AI proposed in Fig. 1b, directly managing the open-loop response of the same circuit. The feedback structure is disconnected in a suitable reference plane and the open-loop transfer function is designed looking at the S-parameters of the same network. In this way, it is possible to determine the proper characteristics of the closed-loop circuit, in order to achieve the desired inductive behavior of the complete structure. This approach allows transferring the design of a single port network with a feedback loop, to that of a double dipole network, so allowing the definition of a systematic synthesis approach.

As a feasibility demonstration, the proposed approach has been applied to the design of an AI for the implementation of a low-power, single-cell bandpass filter at 730 MHz, already proposed in [20]. The design approach for the above-mentioned filter has been also presented and discussed in other previous works [21]–[23]. The filter shows a 3 dB bandpass of 50 MHz and a P1dB compression point of 12 dBm with a quiescent power consumption of only 1 mW. Measurements results are in good agreement with simulations demonstrating the reliability of the proposed design method.

The work is organized as follows. In Section II, the AI synthesis approach is presented; in Section III, a case study is illustrated with the design of an active inductor, reporting test and measurements results on a simple LC-filter, while in Section IV conclusions are drawn.

## II. THE AI SYNTHESIS METHOD

A grounded active inductor is an active, one-port, electric network, whose input impedance is equivalent to that provided by a passive shunt inductor in a limited frequency range [19]. Considering, for instance, the simplified electrical scheme in Fig. 2, the combined operation of an inverting gain stage and a suitable delay network allow obtaining the desired phase shift between input current and voltage. In this case, by using an ideal RC network and modeling the inverting amplifier with a simple voltage-controlled current source, the input impedance can be easily evaluated defining the expression of the input current (equation (1)) and it is shown in (2).

$$\begin{aligned} I_{in} &= I_{delay\ network} + g_m V_1 \\ &= V_{in}\frac{j\omega C}{1+j\omega RC} + V_{in}\frac{g_m}{1+j\omega RC} \end{aligned} \tag{1}$$

$$\begin{aligned} Z_{in} &= \frac{V_{in}}{I_{in}} = \frac{1+j\omega RC}{g_m+j\omega C} \\ &\Longrightarrow Re\,[Z_{in}] + j\cdot Im\,[Z_{in}] \\ &= \frac{g_m+\omega^2 RC^2}{g_m^2+\omega^2 C^2} + j\frac{\omega RCg_m-\omega C}{g_m^2+\omega^2 C^2} \end{aligned} \tag{2}$$

From (2), by fixing $\omega_0$, it is possible to evaluate the proper values for $R$, $C$, and gm in order to obtain the desired inductance level and minimizing, at the same time, losses.

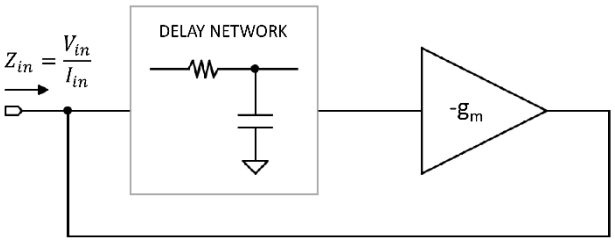


**FIGURE 2.** Ideal representation of an active inductor.

Anyway, while this approach is suitable for simple and ideal networks, it cannot be applied considering real components and distributed elements, as usually happens in practical applications. Also considering parasitics of the transistors, equation (2) becomes even more complex and de facto useless because it is no more trivial to obtain suitable design parameters. In addition, the description of the circuit in terms of voltages and currents is strictly dependent on the considered circuit topology.

In this perspective, a different synthesis method is here proposed; it is based on a conformal transformation of the AI circuit and an equivalent description is carried out by means of Scattering parameters.

Considering the AI general structure, as for instance in Fig. 1a, a symbolic representation of the AI can be arranged by means of traditional n-port network formalism as in Fig. 3a. The "two-port network" block embeds the series connection of the gain stage and the phase shift network, while the input and output ports of the double-dipole are shorted to realize the feedback connection. This circuit, according to the graph theory and waves formalism [24], [25], can be further described as in Fig. 3b.

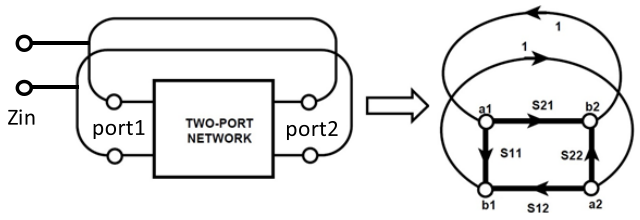


**FIGURE 3.** Generic representations of an AI with a double-dipole network (a) and waves formalism (b).

The proposed descriptive scheme in Fig. 3b (presented again in Fig. 4a) is suitable for some convenient manipulations described as follows.

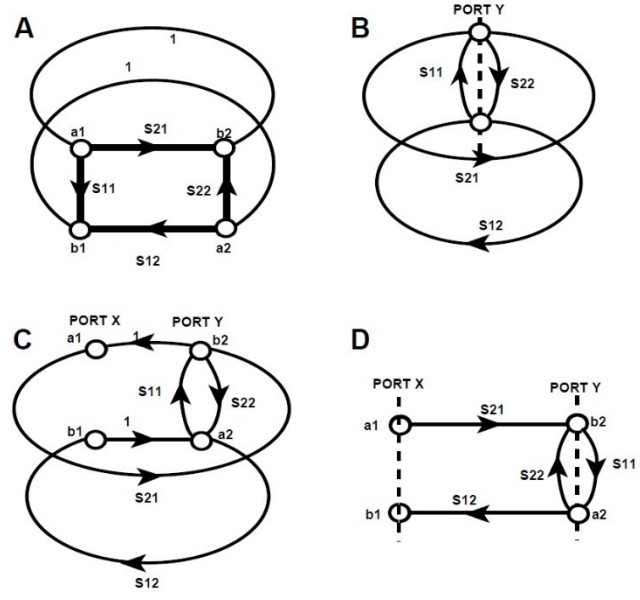


**FIGURE 4.** Graph transformation.

Port 1 and port 2 in the AI architecture are shorted and so may be considered as a single electrical port; this means that in the graph theory they can collapse in a single port as shown in Fig. 4b, where Port $Y$ is introduced. Now considering the aim to obtain an open-loop representation of the circuit, Port $Y$ is paired with a second, virtual, port defined in the feedback loop and named Port $X$, as shown in Fig. 4c. It is important to remark that the latter is not a physical port, but the choice is useful to obtain a proficient transfer function of the AI without perturbing the overall characteristics of the circuit. Thanks to the introduction of Port $X$ and without loss of generality, the circuit can now be analyzed as a double-dipole network, whose equivalent representation is that provided in Fig. 4d. The graph in Fig. 4d represents a more suitable structure with respect to the original description provided in Fig 3b to analyze the open-loop AI transfer function.

The generic transmission coefficients $\rho$ can be easily obtained by applying the Mason rule [22] between two nodes of the graph and evaluated by means of (3).

$$\rho = \frac{P_1\left[1 - \sum L(1)^{(1)} + \sum L(2)^{(1)} - \ldots\right]}{1 - \sum L\,(1) + \sum L\,(2) - \sum L\,(3) + \ldots} + \frac{P_2\left[1 - \sum L(1)^{(2)} + \sum L(2)^{(2)} - \ldots\right]}{1 - \sum L\,(1) + \sum L\,(2) - \sum L\,(3) + \ldots} + \ldots \quad (3)$$

In (3), the $P$ coefficients ($P1$, $P2$, etc.) are all possible paths within the graph that connect the two nodes (or ports). The term $\sum L(2)^{(1)}$ represents the sum of all second-order closed-loop paths in the graph, that don't intersect path 1, which means that they haven't any common nodes or branches with the path 1. Similarly, $\sum L(1)^{(2)}$ represents the sum of all first-order loops that don't intersect the path number 2, and so on. The denominator of (3), also called determinant, does not depend on the selected nodes, but it is a function of the geometry of the considered graph. The generic $\sum L(..)$ term has the same description of the corresponding term at the numerator, but also considering the paths first excluded. By applying this rule, the transmission coefficients assume the expressions in (4) and (5), respectively.

$$\frac{b_Y}{a_X} = \frac{S_{21}}{1 - S_{11} \cdot S_{22}} \quad (4)$$

$$\frac{b_X}{a_Y} = \frac{S_{12}}{1 - S_{11} \cdot S_{22}} \quad (5)$$

The complete transfer function can be obtained by subtracting (5) from (4):

$$G = \frac{b_Y}{a_X} - \frac{b_X}{a_Y} = \frac{S_{21} - S_{12}}{1 - S_{11} \cdot S_{22}} \quad (6)$$

Anyway, in (6), the main contribution is accountable to the $S_{21}$ term, since the real network here considered embeds an active device that is a non-reciprocal element, so the reverse transmission $S_{12}$ may be neglected without loss of generality. With this assumption, the open-loop transfer function $G$ assumes the final expression reported in (7):

$$G = \frac{b_Y}{a_X} - \frac{b_X}{a_Y} \approx \frac{S_{21}}{1 - S_{11} \cdot S_{22}} \quad (7)$$

Considering a small S12, Eq. (7) is similar to that shown in [26] and obtained with a different approach analyzing the design of oscillators.

From (7), it is possible to define the desired conditions for the closed-loop network, in order to achieve an inductive behavior at the input port of the closed-loop AI structure. In fact, by using the conformal transformations above described, the open-loop transfer function corresponds to the reflection coefficient seen at the input port of the closed-loop graph (Fig. 3a), and it finds a counterpart in the AI general structure of Fig. 1b.

The input reflection coefficient $\Gamma$ of the AI block scheme in Fig. 1a can be easily obtained considering the input impedance $Z_{in}$ and the characteristic impedance of the circuit $Z_0$, as shown in (8):

$$\Gamma = \frac{Z_{in} - Z_0}{Z_{in} + Z_0} \tag{8}$$

By considering $\Gamma|_{closed-loop} = G|_{open-loop}$,noting that the open-loop transmission coefficient $G$ corresponds to the reflection coefficient $\Gamma$ at the input port of the closed-loop circuit (as long as the impedance matching condition at ports $X$ and $Y$ with respect to the reference impedance is verified) and imposing an inductive behavior on the input impedance at the desired frequency, it is possible to obtain the proper condition for the transfer function $G$ in the open-loop two-ports configuration. In the Laplace domain, imposing the generic input impedance $Z_{in}$ equal to "$j\omega L$", eq. (8) can be re-arranged as follow:

$$\begin{aligned} G &= \frac{Z_{in} - Z_0}{Z_{in} + Z_0} = \frac{j\omega L - Z_0}{j\omega L + Z_0} = \frac{j\omega L - Z_0}{j\omega L + Z_0} \cdot \frac{j\omega L - Z_0}{j\omega L - Z_0} \\ &= \frac{\omega^2 L^2 + j2Z_0\omega L - Z_0^2}{Z_0^2 + \omega^2 L^2} \\ &= \frac{\omega^2 L^2 - Z_0^2}{Z_0^2 + \omega^2 L^2} + j\frac{2Z_0\omega L}{Z_0^2 + \omega^2 L^2} \end{aligned} \tag{9}$$

The expression in (9) can be better managed if organized highlighting the magnitude and phase of the transmission coefficient $G$. They are reported in the following eqs. (10) and (11), respectively.

$$\begin{aligned} |G| &= \sqrt{\frac{(\omega L)^4 + Z_0^4 - 2(Z_0\omega L)^2 + 4(Z_0\omega L)^2}{\left(Z_0^2 + \omega^2 L^2\right)^2}} \\ &= \sqrt{\frac{(\omega L)^4 + Z_0^4 + 2(Z_0\omega L)^2}{\left(Z_0^2 + \omega^2 L^2\right)^2}} \\ &= \sqrt{\frac{\left(Z_0^2 + \omega^2 L^2\right)^2}{\left(Z_0^2 + \omega^2 L^2\right)^2}} = 1 \end{aligned} \tag{10}$$

$$\angle(G) = \tan^{-1}\left(\frac{2Z_0\omega L}{\omega^2 L^2 - Z_0^2}\right) \tag{11}$$

These equations allow setting the desired behaviour of the transfer function. In particular, the magnitude of the transmission coefficient in (10) should be equal to 1 in order to minimize losses, while its phase, accordingly to the Bode plot of Eq. (9) must rely on the range $(0 \div 180)$ degree to obtain an inductive behavior, as shown in Fig. 5. The equation (10) derives from an ideal situation where the considered inductance $L$ has no resistive part and constitutes the optimal design condition for the active inductor to achieve a high (ideally infinite) quality factor. It can be easily demonstrated that, by adding a resistor to the definition of the inductor impedance in (10), the modulus of the transfer function $G$ will be less than one and frequency-dependent.

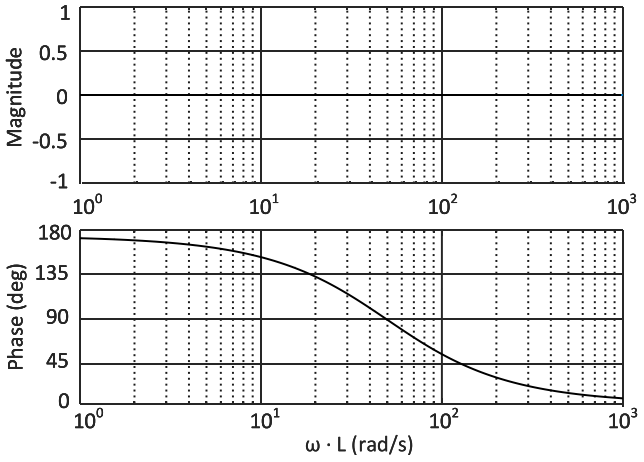


**FIGURE 5.** Bode plot of an ideal inductor.

In summary, in order to achieve an inductive behavior at the input port once the feedback loop is closed, the transfer function $G$ should verify the following conditions in the desired frequency range:

$$|G(\omega)| = \left|\frac{S_{21}}{1 - S_{11} \cdot S_{22}}\right| \leq 1 \tag{12}$$

$$180^\circ \geq \angle[G(\omega)] = \angle\left(\frac{S_{21}}{1 - S_{11} \cdot S_{22}}\right) \geq 0^\circ \tag{13}$$

In (12) the modulus of G should be equal or less than one at the frequency of operation, but, since there is an active amplifier in the loop, it is mandatory to not exceed the unity. A designer has to be aware that, by approaching the unity for the modulus of G, the technological spread that affects the circuit implementation could cause a malfunction of the system. Therefore, according to the performance requirements, the designer should put the necessary attention on this point.

For the sake of illustration, if a specific inductance value $L_0$ is required, eq. (8) can be arranged as in (14), where $\tau_0$ defines the ratio between $L_0$ and $Z_0$.

$$\Gamma = -\frac{(1 - j\omega\tau_0)}{(1 + j\omega\tau_0)} \tag{14}$$

The two binomial terms in (14) - numerator and denominator - have the same cut-off frequency and they both contribute to a clockwise phase rotation, as it is shown in Fig. 6 for different inductance values.

From a practical point of view, the phase behavior reported in Fig. 6 may be difficult to synthesize, so without loss of generality, its asymptotic diagram can be also considered.

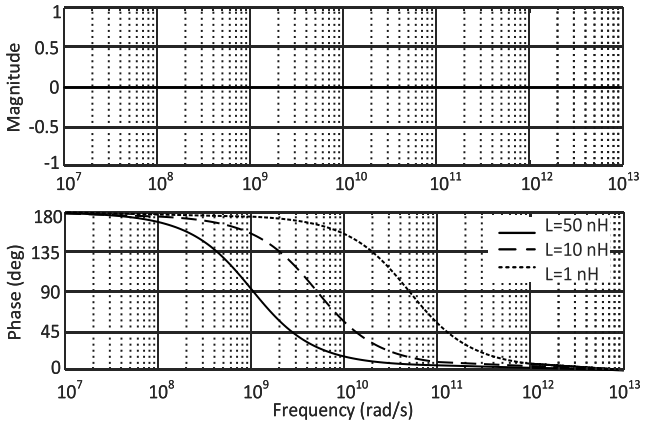


**FIGURE 6.** Bode plot of the active inductor input impedance for different inductance values.

Defining $\omega_t$ as $1/\tau_0$, for $\omega < 0.1\omega_t$, it is assumed that the real part of the binomial terms in (14) is dominant with respect to the imaginary part, thus the phase can be approximated with a constant equal to 180 degrees. In the range $[0.1\omega_t, 10\omega_t]$, the phase can be linearized with a fixed slope segment with a slope equal to $-\pi/2$ *rad/dec*; while for $\omega > 10\omega_t$, the imaginary part becomes prevalent and the phase is again constant and equal to 0 degrees.

As a consequence, the phase condition for the $G$ transmission coefficient which has been already shown in (13) can be re-arranged as in (15):

$$\begin{cases} \angle[G(\omega)] = 180°, & \omega < 0.1\omega_t \\ 180° \geq \angle[G(\omega)] =\geq 0°, & 0.1\omega_t < \omega < 10\omega_t \\ \angle[G(\omega)] = 0°, & \omega > 10\omega_t. \end{cases} \quad (15)$$

Finally, the design algorithm following the proposed method can be summarized as follows:

1) Define the desired inductor parameters (frequency of operation, inductance value);
2) Design the inverting, single transistor amplifier according to the chosen frequency range of operation;
3) Design the compensation network (eventually, adjust the amplifier design parameters) in order to satisfy the equations 12, 14 and 15 for the two-port network constituted by the amplifier and the compensation network. The microstrip dimensions and length of the final arrangement (including the length of the feedback loop connection) should be considered at this stage;
4) Close the loop, achieving a one-port schematic, and verify the input impedance of the active inductor.

It is important to notice, that it is not trivial to obtain an inductive behavior with an active equivalent solution at all frequencies. A classical solution consists of enforcing the desired inductive impedance only in the operative bandwidth or, at least, nearby the operational frequency. In these cases, the provided conditions, necessary to achieve an inductive impedance, can be satisfied only in a limited frequency range without loss of generality.

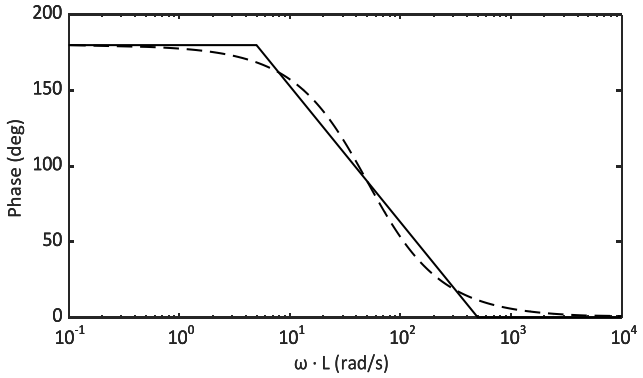


**FIGURE 7.** Asymptotic approximation (dashed line) of the phase diagram (solid line) of the AI.

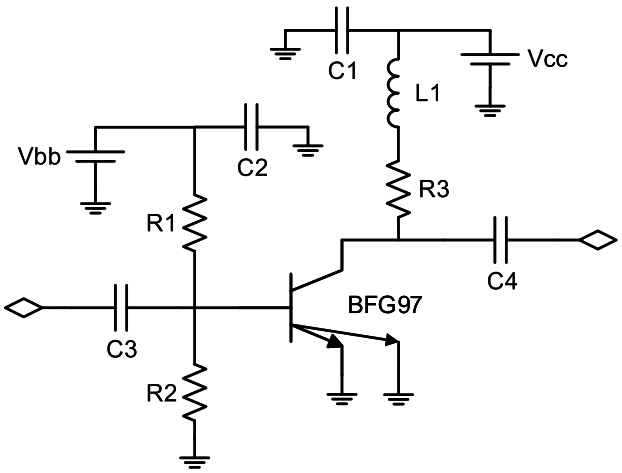


**FIGURE 8.** Schematic of the considered, low-power, inverting amplifier, as depicted in [20]. 

## III. EXAMPLE OF APPLICATION

As illustrated in the previous Section, the S-parameters in (7) refer to a two-port network which is composed of an inverting amplifier, followed by a passive phase shift network. This allows to carry out the design directly considering the open-loop circuit and focusing the attention on these building blocks. As a first step, the amplifier must be designed with the desired characteristics in terms of power consumption, stability, and dynamic range. As a second step, the phase delay network is defined in order to fulfill the goals relative to the open-loop transfer function $G$. Finally, the feedback loop can be closed checking the AI performance.

As a demonstration of the proposed method, an active inductor design has been considered by applying the AI in a simple resonator, an $LC$ circuit which realizes a low-order bandpass filter [20]–[23].

In particular, the tunable active filter, proposed by the same authors in [20] has been taken into account for this example of application, because of the availability of measurements results.

The already proposed active stage is shown in Fig. 8. It has been realized on a Taconic TLX-8 low-loss substrate with the

BFG97 transistor provided by Infineon. All passive elements are low-losses SMD components. The transistor is biased at 2 V with a quiescent current of only 0.5 mA and this allows to obtain a quiescent power consumption of only 1 mW. Separate collector and base bias pins are used in order to provide the prototype of a tuning capability of the bias current with respect to possible transistor model variations.

In order to obtain a quasi-ideal, equivalent active inductor a passive phase delay network has been introduced in the design as shown in Fig. 1a and with the aim to verify the conditions of eqs. (12) and (13). The complete schematic is shown in Fig. 10. It has been conceived by means of *R-L-C* components. It is important to notice that the use of traditional passive inductors in the AI circuit does not influence the performance achievable by the AI since the AI quality factor, according to eqs. (12) and (13), depends only on the magnitude and phase of the transfer function, that means on the correct phase delay between input current and voltage considering the general scheme of Fig. 1a. In fact, from the typical representation of a generic inductor quality factor $Q_L$, it is possible to achieve the following relationship with the open-loop transfer function $G$ :

$$\mathrm{Q_L} = \frac{\Im\mathfrak{m}\{Z_{in}\}}{\Re\mathfrak{e}\{Zin\}} = \frac{\Im\mathfrak{m}\left\{(1+G)\,/\,(1-G)\right\}}{\Re\mathfrak{e}\left\{(1+G)\,/\,(1-G)\right\}} \tag{16}$$

using the well-known relation $Z_{in} = Z_0\,(1+\Gamma_{in})\,/\,(1-\Gamma_{in})$ and recalling that the closed-loop reflection coefficient $i\Gamma_{in} = \Gamma$ is equal to the open-loop, two-ports network transfer function $G$. By multiplying both numerator and denominator of (16) by the term $|1-G|^2$, the equation becomes:

$$\begin{aligned}\mathrm{Q_L} &= \frac{\Im\mathfrak{m}\left\{1-G^*+G-|G|^2\right\}}{\Re\mathfrak{e}\left\{1-G^*+G-|G|^2\right\}} = \frac{2\cdot\Im\mathfrak{m}\{G\}}{1-|G|^2} \\ &= \frac{2\cdot|G|\sin(G)}{1-|G|^2}\end{aligned} \tag{17}$$

From the denominator of (17), it can be noticed that the quality factor $Q_L$ increases, as soon as the modulus of the transfer function $G$ approaches the unity, while it decreases if $|G|$ tends to 0, or if the term $\angle G$ approaches 0 or $\pi$, at the frequency of operation $\omega = \omega_0$. This is in accordance with eqs. (12), (13) and (15).

Moreover, two varactors (the BBY59 from Infineon) have been included in the delay network and they are useful for tuning purposes in case of possible mismatch problems or model inaccuracies. Clearly, they can be used also to tune the AI characteristics in order to realize a variable component. Fig. 9 illustrates the complete schematic of the AI in open-loop configuration, as previously discussed. The transfer function of this circuit must fulfill eqs. (12) and (13) in order to obtain the desired inductive behavior and inductance value at a fixed frequency.

In this example, Fig. 10 shows the magnitude and phase of $\Gamma = G$ simulated for the complete active inductor, while in Fig. 11 the final layout of the circuit is reported illustrating

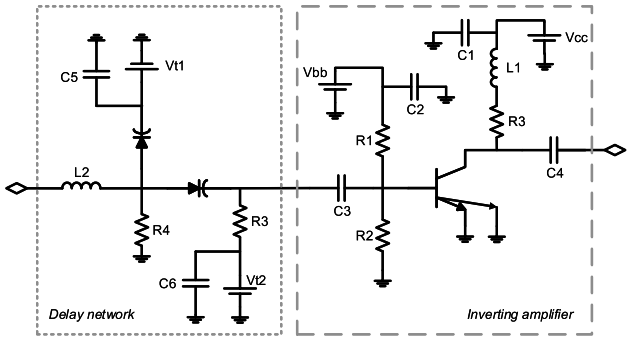


**FIGURE 9.** Schematic of the complete open-loop network of the AI proposed in [20]. ©2017 IEEE. All rights reserved.

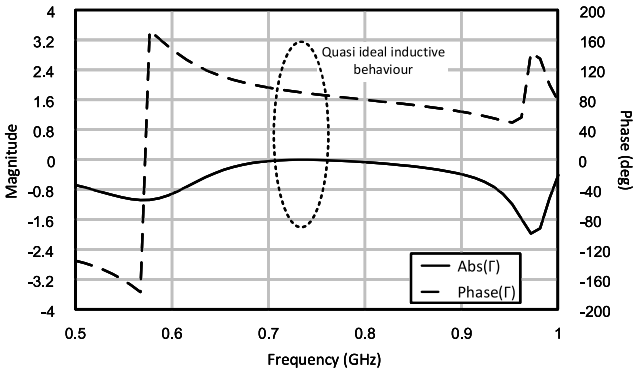


**FIGURE 10.** Magnitude (left) and phase (right) of the two-port open-loop transfer function *G* simulated for the complete active inductor.

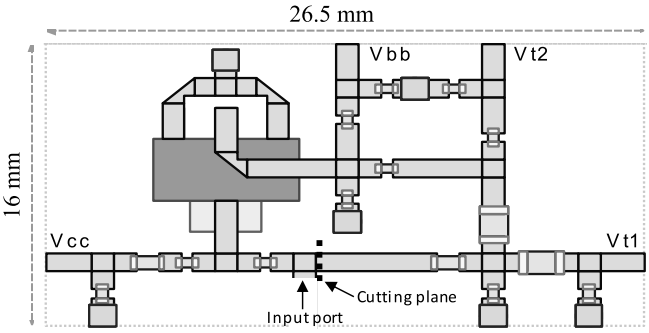


**FIGURE 11.** Layout of the complete active inductor as proposed in [20]. ©2017 IEEE. All rights reserved.

also the considered cutting plane and the input port of the active inductor that has been conceived. From Fig. 10 it can be noticed that in a real case the inductive behaviour can be obtained only in a limited frequency range, where the phase of the complete network tends to 0 from 180 degrees, while the magnitude of the transfer function is close to zero at the desired frequency of 730 MHz. By closing the loop as illustrated in Fig. 3, the equivalent impedance of Fig. 12 has been obtained. As stated, it has an almost ideal inductance behaviour at 730 MHz.

In addition, the simulated quality factor of the designed AI is reported in Fig. 13, comparing it with the quality factor of two commercial High-Q passive inductors from Murata

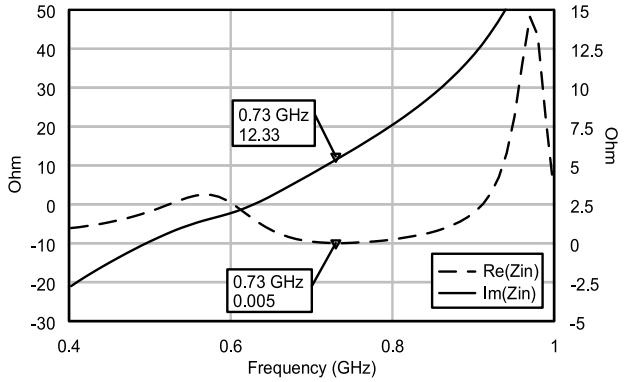


**FIGURE 12.** Input impedance of the active inductor.

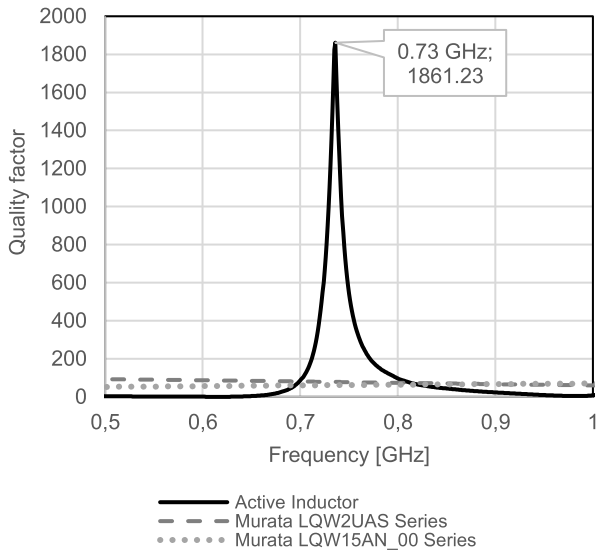


**FIGURE 13.** Quality factor simulation comparison for the designed AI and two commercial passive inductors from Murata Manufacturing Co.

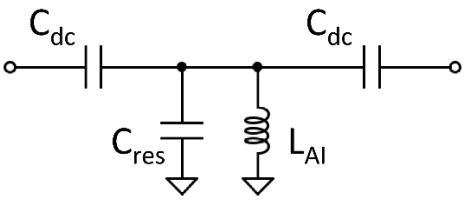


**FIGURE 14.** Schematic of the prototype filter.

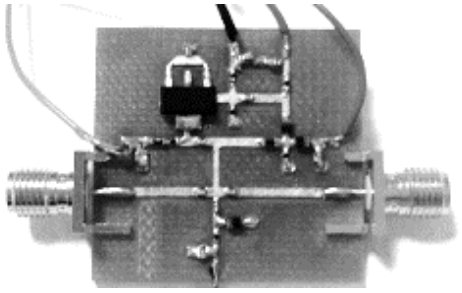

**FIGURE 15.** The implemented prototype of the single-cell bandpass filter based on active inductor.

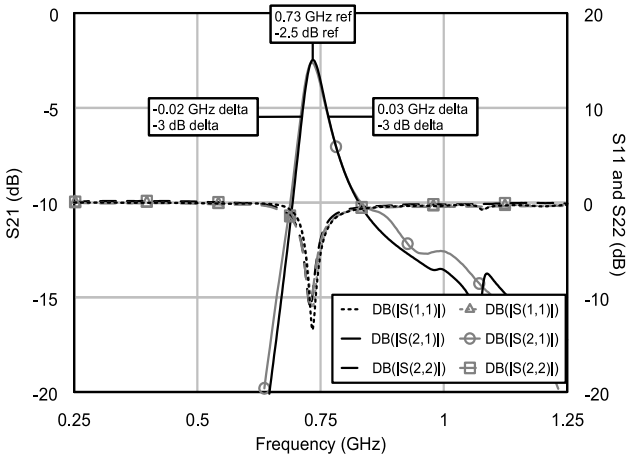


**FIGURE 16.** Linear analysis of the test circuit: Simulated (black lines) and measured (grey lines) S-parameters. [20] ©2017 IEEE. All rights reserved.

Manufacturing Company. It can be noticed that the Q of the custom AI exceeds a value of 1800 at the frequency of operation, underlining the great advantages of AI with respect to passive solutions.

Tests have been performed including the designed active inductor in a simple *LC*-filter obtained resonating the AI with a shunt capacitor, as shown in Fig. 14. $C_{res}$ is the resonating capacitance, while $C_{dc}$ are decoupling capacitors. The use of the AI in this structure enhances the filter behaviour thanks to the high-quality factor of the active circuit that has been introduced. This prototype has been fabricated on the same substrate, the TLX8, and by using similar SMD components to those employed for the AI simulation.

In Fig. 15 the implemented prototype of the single-cell bandpass filter, AI-based, is depicted, while in Fig. 16 the S parameters of the single-cell filter are reported considering both simulations and measurements. The experimental results confirm the validity of the proposed method for Ai design by means of conformal transformation.

As expected, the −3 dB bandwidth is about 50 MHz, for a relative bandwidth of about 6.8%. The filter insertion loss is 2.5 dB at the central frequency, while both input and output matchings are below −10 dB at the same frequency. The DC power consumption of the circuit is 1 mW since the prototype requires a bias current of 0.5 mA in the small-signal regime, as simulated.

## IV. CONCLUSION

A novel design method for the definition and synthesis of active inductors is here proposed. The analysis is carried out by means of S-parameters and conformal transformations defined by using the Graph Theory. In this way, it is possible to define the characteristics of a closed-loop circuit (that is the architecture of an active inductor) analyzing it as a double-dipole network, so simplifying the design process.

An example of application has been also provided and the conceived AI has been tested on a simple *LC*-resonator that acts as a bandpass circuit. Results show the feasibility of the proposed approach for the AIs design.

## REFERENCES

[1] C. F. Campbell and R. J. Weber, "Design of a broadband microwave BJT active inductor circuit," in *Proc. 34th Midwest Symp. Circuits Syst.*, vol. 1, May 1991, pp. 407–409, doi: 10.1109/MWSCAS.1991.252183.

[2] D. P. Anderson, R. J. Weber, and S. F. Russell, "Bipolar active inductor realizability limits, distortion, and bias considerations," in *Proc. 39th Midwest Symp. Circuits Syst.*, vol. 1, Aug. 1996, pp. 241–244.

[3] Y. Zhao, W. Zhang, H. Xie, D. Gao, and Q. Fu, "An improved active inductor with tunable active resistor feedback and multi-regulated cascode circuit," *Sensors Transducers*, vol. 172, no. 6, pp. 191–195, Jun. 2014.

[4] S. Hara, T. Tokumitsu, and M. Aikawa, "Lossless broad-band monolithic microwave active inductors," *IEEE Trans. Microw. Theory Techn.*, vol. 37, no. 12, pp. 1979–1984, Dec. 1989.

[5] Y. Wu, X. Ding, M. Ismail, and H. Olsson, "RF bandpass filter design based on CMOS active inductors," *IEEE Trans. Circuits Syst. II, Analog Digit. Signal Process.*, vol. 50, no. 12, pp. 942–949, Dec. 2003.

[6] F. Yuan, *CMOS Active Inductors and Transformers*, 1st ed. Berlin, Germany: Springer, 2008.

[7] A. Thanachayanont and S. S. Ngow, "Class AB VHF CMOS active inductor," in *Proc. 45th Midwest Symp. Circuits Syst. (MWSCAS)*, vol. 1, Aug. 2002, pp. 64–67.

[8] A. Ghadiri and K. Moez, "Wideband active inductor and negative capacitance for broadband RF and microwave applications," *IEEE Trans. Compon., Packag., Manuf. Technol.*, vol. 4, no. 11, pp. 1808–1814, Nov. 2014.

[9] J. Koo, B. An, and Y. Jeong, "Wideband CMOS high-Q 2-port active inductor using parallel LC resonance circuit," in *Proc. Asia–Pacific Microw. Conf. (APMC)*, New Delhi, India, Dec. 2016, pp. 1–4, doi: 10.1109/APMC.2016.7931303.

[10] J. Ou, "Design considerations of CMOS active inductor for low power applications," in *Proc. IEEE Dallas Circuits Syst. Conf. (DCAS)*, Arligton, TX, USA, Oct. 2016, pp. 1–4.

[11] D. C. Hamill, "Lumped equivalent circuits of magnetic components: The gyrator-capacitor approach," *IEEE Trans. Power Electron.*, vol. 8, no. 2, pp. 97–103, Apr. 1993.

[12] A. Ben Hammadi, F. Haddad, M. Mhiri, S. Saad, and K. Besbes, "RF and microwave reconfigurable bandpass filter design using optimized active inductor circuit," *Int. J. RF Microw. Comput.-Aided Eng.*, vol. 28, no. 9, Nov. 2018, Art. no. e21550, doi: 10.1002/mmce.21550.

[13] R. Mehra, V. Kumar, A. Islam, and B. K. Kaushik, "Variation-aware widely tunable nanoscale design of CMOS active inductor-based RF bandpass filter," *Int. J. Circuit Theory Appl.*, vol. 45, no. 12, pp. 2181–2200, Dec. 2017, doi: 10.1002/cta.2364.

[14] G. Leuzzi, V. Stornelli, L. Pantoli, and S. Del Re, "Single transistor high linearity and wide dynamic range active inductor," *Int. J. Circuit Theory Appl.*, vol. 43, no. 3, pp. 277–285, 2013, doi: 10.1002/cta.1938.

[15] L. Pantoli, V. Stornelli, and G. Leuzzi, "Tunable active filters for RF and microwave applications," *J. Circuits, Syst. Comput.*, vol. 23, no. 6, Jul. 2014, Art. no. 1450088.

[16] V. Stornelli, L. Pantoli, and G. Leuzzi, "High quality factor L-band active inductor-based band-pass filters," *J. Circuits, Syst. Comput.*, vol. 22, no. 3, Mar. 2013, Art. no. 1350014.

[17] L. Pantoli, V. Stornelli, and G. Leuzzi, "A low-voltage low-power 0.25 $\mu$m integrated single transistor active inductor-based filter," *Anal. Integr. Circuits Signal Process.*, vol. 87, no. 3, pp. 463–469, Jun. 2016.

[18] P. Colucci, G. Leuzzi, L. Pantoli, and V. Stornelli, "Third order integrable UHF bandpass filter using active inductors," *Microw. Opt. Technol. Lett.*, vol. 54, no. 6, pp. 1426–1429, Jun. 2012.

[19] L. Pantoli, G. Leuzzi, and V. Stornelli, "Class AB tunable active inductor," *Electron. Lett.*, vol. 51, no. 1, pp. 65–67, Jan. 2015.

[20] L. Pantoli, V. Stornelli, and G. Leuzzi, "High efficiency active filter," in *Proc. Integr. Nonlinear Microw. Millimetre-Wave Circuits Workshop (INMMiC)*, Graz, Austria, Apr. 2017, pp. 1–3, doi: 10.1109/INMMIC.2017.7927303.

[21] A. Leoni, L. Pantoli, Z. Marinkovic, V. Stornelli, and G. Leuzzi, "An approach for AI-based filter design by means of neural networks," in *Proc. 13th Int. Conf. Adv. Technol., Syst. Services Telecommun. (TELSIKS)*, Nis, Serbia, Oct. 2017, pp. 343–346, doi: 10.1109/TELSKS.2017.8246294.

[22] A. Leoni, L. Pantoli, V. Stornelli, G. Leuzzi, and Z. Marinkovic, "Automated calibration system for RF configurable voltage-controlled filters," *IEEE Trans. Circuits Syst. II, Exp. Briefs*, vol. 65, no. 8, pp. 1034–1038, Aug. 2018, doi: 10.1109/TCSII.2018.2790078.

[23] A. Leoni, L. Pantoli, V. Stornelli, G. Leuzzi, and Z. Marinkovic, "Active filters tuning interface," in *Proc. Int. Conf. IC Design Technol. (ICICDT)*, Otranto, Italy, Jun. 2018, pp. 69–72, doi: 10.1109/ICICDT.2018.8399758.

[24] D. M. Pozar, *Microwave Engineering*, 4th ed. Hoboken, NJ, USA: Wiley, 2012, Ch. 4.

[25] N. Munro and P. D. Mcmorran, "Signal-flow-graph reduction, Mason's rule and the system matrix," *Electron. Lett.*, vol. 6, no. 23, pp. 752–754, 1970.

[26] M. Randall and T. Hock, "General oscillator characterization using linear open-loop S-parameters," *IEEE Trans. Microw. Theory Techn.*, vol. 49, no. 6, pp. 1094–1100, Jun. 2001.

**ALFIERO LEONI** (Member, IEEE) was born in L'Aquila, Italy. He received the master's (Laurea) degree *(cum laude)* in electronic engineering, in 2016, and the Ph.D. degree from the Department of Industrial and Electronic Engineering, University of L'Aquila, in February 2020. Several months before his master's (Laurea) degree, he joined as an External Collaborator at the Department of Industrial and Electronic Engineering, University of L'Aquila. He is currently a Research Fellow with the Department of Industrial and Electronic Engineering, University of L'Aquila. His research interests include the design of analog electronic circuits and systems for energy harvesting, industrial, and microwave applications. He acts as a Reviewer for several international journals and conferences.

**VINCENZO STORNELLI** (Senior Member, IEEE) was born in Avezzano, Italy. He received the Laurea degree *(cum laude)* in electronic engineering, in 2004. In October 2004, he joined the Department of Electronic Engineering, University of L'Aquila, L'Aquila, Italy, where he is currently an Associate Professor. His research interests include several topics in computational electromagnetics, including microwave antenna analysis for outdoor ultrawideband applications. He serves as a Reviewer for several international journals. He serves as an Editor for the *Journal of Circuits, Systems, and Computers*.

**LEONARDO PANTOLI** (Member, IEEE) received the degree *(cum laude)* in electronic engineering and the Ph.D. degree in electrical and information engineering from the University of L'Aquila, L'Aquila, Italy, in 2006 and 2010, respectively. From 2007 to 2008, he spent several months with the Communications Engineering Department, University of Cantabria, Spain, and the C2S2 Department, XLIM Research Institute, Brive La Gaillarde, France. He is currently a Researcher with the University of L'Aquila. His research interests include the development of methods and algorithms for the design of RF and microwave nonlinear circuits, stability analysis under large-signal regime, active filters, and MMICs design.

**GIORGIO LEUZZI** received the degree *(cum laude)* in electronic engineering from the University of Rome, La Sapienza, Italy, in 1982. In 1984, he became a Teaching and Research Assistant with the University of Rome, Tor Vergata, Italy, where he has been teaching microwave electronics, since 1991. He became an Associate Professor and a Full Professor of electronic devices with the University of L'Aquila, Italy, in 1998 and 2001, respectively. His research interests include the simulation of semiconductor devices for microwaves and millimeter waves, the linear and nonlinear characterization of microwave and millimeter-wave active devices, and the development of methods and algorithms for microwave nonlinear circuit design.

**ZLATICA MARINKOVIC** (Senior Member, IEEE) graduated from the Faculty of Electronic Engineering, University of Niš, Serbia, in 1999. She received the M.Sc. and Ph.D. degrees in telecommunications from the University of Niš, in 2003 and 2007, respectively. She is currently an Associate Professor with the Faculty of Electronic Engineering, University of Niš. Her main research interests include microwave electronics and artificial neural networks and their application in the field of microwaves and telecommunications. She serves as the IEEE MTT-S Undergraduate Scholarship Chair and the Secretary of IEEE MTT-S Chapter of Serbia and Montenegro. She was the Editor-in-Chief of the journal *Microwave Review*, a publication of Serbian Society for Microwave Techniques, Technologies and Systems, and Serbia and Montenegro IEEE MTT-S Chapter.